AIAA AVIATION Forum
12-16 June 2023, San Diego, CA and Online
AIAA AVIATION 2023 Forum

10.2514/6.2023-3709

Noise amplification in hypersonic blunt body flows

Anubhav Dwivedi
Ming Hsieh Department of Electrical and Computer Engineering, University of Southern California

Mihailo R. Jovanović
Ming Hsieh Department of Electrical and Computer Engineering, University of Southern California

We utilize stochastically-forced compressible linearized Navier-Stokes equations to study the dynamics of hypersonic flows over blunt bodies. Our analysis of the energy of the flow fluctuations around the laminar stagnated flow reveals strong amplification in the presence of background noise. We also provide insights into how changes in different physical parameters, such as the temperature of the blunt body and its curvature, influence the amplification of flow fluctuations. We show that increasing the bluntness and decreasing the wall temperature can significantly enhance the fluctuation amplification. In addition, we also evaluate the global response in the presence of localized sources of stochastic excitations such as those associated with surface roughness. Our approach reveals substantial amplification of flow fluctuations along the convexly curved surface of the blunt leading edges and suggests that amplification of these stochastic excitation sources (e.g., free-stream turbulence and surface roughness) that are unavoidable in experiments might play a crucial role in transition observed over such geometries.

Downloaded by University of Southern California on December 22, 2023 | http://arc.aiaa.org | DOI: 10.2514/6.2023-3709

I. Introduction

Vehicle surface heating at hypersonic flow conditions is a major concern: an unmanaged thermal loading on vehicle surface can lead to structural failure. Throughout the flight geometry, the largest amount of heating typically appears at the nose-tip of the flight vehicle, where the high-speed flow undergoes a rapid deceleration [1]. A common approach to reduce this heat flux is to increase the bluntness by decreasing the curvature of the nose-tip [2]. However, experiments in wind-tunnels indicate that such an arbitrary increase in the bluntness can cause an early transition of the downstream boundary layer from a laminar to a turbulent state [3, 4]. The onset of turbulence introduces an additional source of significant aerodynamic heating [5] and the role of nose-tip bluntness in initiating this transition process is required.

The early onset of flow transition in the blunt body flows at hypersonic conditions has been a subject of numerous experimental [6, 7] and numerical investigations [8, 9]. The classical approach to understanding transition onset involves carrying out a spectral (i.e. normal mode) analysis of the linearized compressible flow equations. In this framework, if given flow conditions lead to unstable normal modes then the linearized dynamical generator associated with the laminar flow is also unstable. However, previous applications of the hydrodynamic stability analysis [10] indicate that the an increase in nose bluntness causes a decrease in the growth of these unstable modes in the boundary layer [11, 12], eventually leading to stabilization of these modes. Interestingly, this observation is in contrast with the experimental observations that indicate an earlier onset of flow transition with an increase in bluntness [4, 7, 13]. Recently, it has been recognized that even in stable laminar flows, transient (finite-time) growth can play significant role [14, 15] in the transition process. This approach has been utilized to identify the 'worst case' initial state in the blunt body flows [16–18] that can lead to the largest energy growth of flow fluctuations. However, these initial states may not be realizable in experiments. Furthermore, this analysis does not account for uncertainty encountered in realistic setups. In this context, an input-output approach that can account for the influence of external disturbances provides a valuable framework for analyzing the influence of the unmodeled dynamics.

A major source of uncertainty in the experiments over blunt bodies appears in the form of distributed roughness at the nose tip [4, 19]. Experimental observations indicate that the onset of transition on blunt cones are extremely sensitive to the surface finish near the stagnation region [4]. In the present work, utilize an input-output framework that models the dynamical influence of surface roughness as small amplitude white-in-time external disturbances. These disturbances are considered as inputs, while the fluctuation velocities and temperature are considered as outputs. In particular, we consider the experiments carried out by Borovoy *et al.* [13] over blunted flat plates in a Mach 5 free stream.

Input-output (I/O) analysis that evaluates the response (outputs) of the linearized Navier-Stokes (NS) equations to external perturbation sources (inputs) was successfully employed to quantify the amplification and study transition

Copyright © 2023 by Anubhav Dwivedi. Published by the American Institute of Aeronautics and Astronautics, Inc., with permission.

mechanisms in low speed channels [20–22], boundary layers [23–26], jets [27] and hypersonic shock-boundary-layer-interactions [28–31]. However, quantifying the role of stochastic disturbance sources in high-speed flows is still an open challenge due to the large computational costs associated with the obtaining the fluctuations associated with the various realization of the disturbances in a spatially evolving flow field. In this paper, we utilize the I/O analysis to demonstrate that the hypersonic flow over blunt flat plates strongly amplify external stochastic excitations with a specific spanwise length scale. Our approach indicates that in the presence of background noise close to the surface, increasing the leading edge bluntness causes a substantial increase in the fluctuation amplification near the stagnation region which is found to agree well with experimentally observed trends.

Our presentation is organized as follows. In § II, we present the linearized model and provide a brief summary of the I/O formulation in the presence of stochastic disturbances. In § III, we evaluate the energy amplification in a locally parallel stagnation boundary layer flow in the presence of background noise. We also quantify the role of physical parameters such as nose-bluntness and wall temperature on the robustness of the laminar hypersonic flow. § IV we evaluate the global response of 2D laminar hypersonic base flow over flat plate with cylindrical leading edges in the presence of stochastic disturbances that are present close to the wall. We demonstrate the dependence of the fluctuation energy on the radius of curvature of leading edge. We conclude our presentation in § V.

Downloaded by University of Southern California on December 22, 2023 | http://arc.aiaa.org | DOI: 10.2514/6.2023-3709

II. Linearized model for compressible flows

The compressible NS equations for perfect gas in conservative form are given by

$$\frac{\partial \mathbf{U}}{\partial t} + \frac{\partial \mathbf{F}_j}{\partial x_j} = 0, \tag{1}$$

where $\mathbf{F}_j(\mathbf{U})$ is the flux vector and $\mathbf{U} = \big(\rho, \rho\mathbf{u}, E\big)$ is the vector of conserved variables representing mass, momentum, and total energy per unit volume of the gas [32]. We decompose the state vector $\mathbf{U}(\mathbf{x}, t)$ into a steady base component $\overline{\mathbf{U}}(\mathbf{x})$ and a time-varying perturbation component $\mathbf{U}'(\mathbf{x}, t)$, $\mathbf{U}(\mathbf{x}, t) = \overline{\mathbf{U}}(\mathbf{x}) + \mathbf{U}'(\mathbf{x}, t)$. The evolution of small perturbations is then governed by the linearized flow equations,

$$\frac{\partial}{\partial t}\mathbf{U}'(\mathbf{x}, t) = \mathcal{A}(\overline{\mathbf{U}})\mathbf{U}'(\mathbf{x}, t), \tag{2}$$

where $\mathcal{A}(\overline{\mathbf{U}})$ represents the compressible NS operator resulting from linearization of (1) around the base flow $\overline{\mathbf{U}}$. We assume that $(\rho\mathbf{u})'$ satisfies homogeneous Dirichlet boundary conditions while ρ' and E' satisfy homogeneous Neumann boundary conditions at the wall. Along the rest of the boundaries, all the perturbations are assumed to satisfy homogeneous Dirichlet boundary conditions. A second order central finite volume discretization (as described in [33]) is used to obtain the finite dimensional approximation of Eq. (2),

$$\frac{\mathrm{d}}{\mathrm{d}t}\bar{\mathbf{q}} = \bar{\mathbf{A}}\bar{\mathbf{q}}, \tag{3}$$

which describes the dynamics of the spatially discretized perturbation vector $\bar{\mathbf{q}} \in \mathbb{C}^{5N\times 1}$, where N denotes the number of finite volume cells used to discretize the flow domain.

In this paper, we are interested in quantifying the amplification of exogenous disturbances in boundary layer flows [21, 34]. To accomplish this objective, we augment the evolution model (3) with external excitation sources

$$\begin{aligned} \frac{\mathrm{d}}{\mathrm{d}t}\bar{\mathbf{q}} &= \bar{\mathbf{A}}\bar{\mathbf{q}} + \bar{\mathbf{B}}\bar{\mathbf{f}}, \\ \bar{\boldsymbol{\phi}} &= \bar{\mathbf{C}}\bar{\mathbf{q}}, \end{aligned} \tag{4}$$

where $\bar{\mathbf{f}}$ is a spatially distributed and temporally varying disturbance source (input) and $\bar{\boldsymbol{\phi}} = (\rho', \mathbf{u}', T')$ is the quantity of interest (output), where T' denotes temperature perturbations. In Eq. (4) the matrix $\bar{\mathbf{B}} \in \mathbb{C}^{5N\times d}$ specifies how the input enters into the state equation, while the matrix $\bar{\mathbf{C}} \in \mathbb{C}^{r\times 5N}$ extracts the output from the state $\bar{\mathbf{q}}$. The definition of the input and the output matrices is provided in the appendix.

Figure 1 (a) shows a typical high speed flow over a blunt flat plate obtained from numerical simulations [32]. Since the flow on this geometry is invariant in the spanwise z direction, we can simplify our analysis by taking Fourier transform in the spanwise direction. This enables a normal-mode representation of the forcing $\bar{\mathbf{f}}$ and the state $\bar{\mathbf{q}}$,

$$\bar{\mathbf{f}}(x, y, z, t) = \hat{\mathbf{f}}(x, y, t)\, e^{\mathrm{i}k_z z}, \quad \bar{\mathbf{q}}(x, y, z, t) = \hat{\mathbf{q}}(x, y, t)\, e^{\mathrm{i}k_z z}. \tag{5}$$

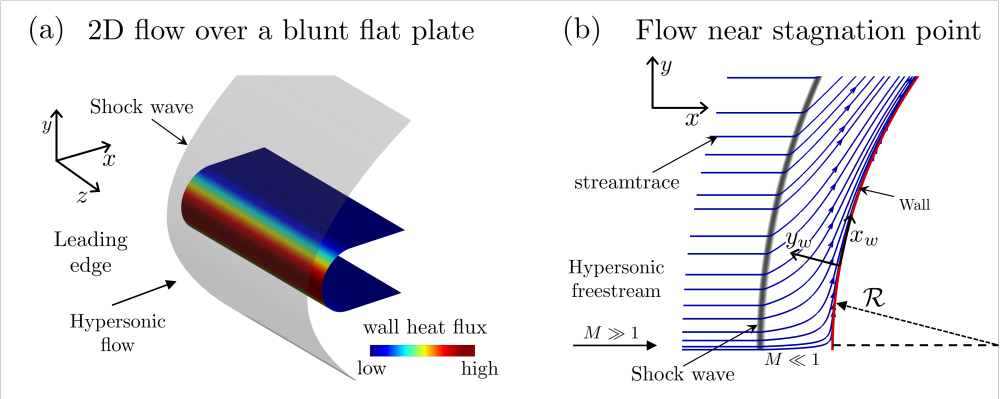

Fig. 1 Schematic of a high speed flow over a blunt flat plate: (a) spanwise homogeneous base flow heat flux into the vehicle surface; (b) zoomed in view of the various flow regions around the stagnation point.

As a result, the state space representation given in equation (4) can be parameterized over the spanwise wave number k_z. We will utilize this parameterization throughout the rest of this paper.

A. Change of coordinates

We utilize Chu's [35] compressible energy norm to quantify the amplification of flow fluctuations in the presence of external disturbances. The resulting compressible energy density for an ideal gas can be defined as,

$$\|\mathbf{q}\|_E^2 = \int_\Omega \frac{1}{2}\bar{\rho}(u'^2 + v'^2 + w'^2) + \frac{\bar{p}}{2}\left(\frac{\rho'}{\bar{\rho}}\right)^2 + \frac{\bar{E}_{\text{int}}}{2}\left(\frac{T'}{\bar{T}}\right)^2 \mathrm{d}\Omega, \tag{6}$$

where, Ω denotes the flow domain of interest, $\bar{p}$ denotes the base flow pressure, and $\bar{E}_{\text{int}}$ denotes the base flow internal energy. The energy norm in equation (6) can be expressed as an inner product,

$$E = \langle \mathbf{U}', \mathbf{U}' \rangle_e = \int_\Omega \mathbf{U}'^* \mathbf{Q} \mathbf{U}' \mathrm{d}\Omega =: \langle \mathbf{U}', \mathbf{Q}\mathbf{U}' \rangle, \tag{7}$$

where $\langle \cdot, \cdot \rangle$ denotes the standard L_2 inner product and $\mathbf{Q}$ is the energy weighting matrix. After the finite volume discretization, the energy norm is determined by $E = \bar{\mathbf{q}}^* \mathrm{Q} \bar{\mathbf{q}}$, where Q is the finite-dimensional representation of the operator $\mathbf{Q}$.

Since the matrix Q is positive-definite, the state of the linearized equation (4) can be transformed into a set of coordinates in which the energy is determined by the standard Euclidean norm, i.e., $E = \mathbf{q}^* \mathbf{q}$ with $\mathbf{q} := \mathrm{Q}^{1/2} \bar{\mathbf{q}}$. With this change of coordinates the resulting discretized state space matrices $\bar{\mathbf{A}}$, $\bar{\mathbf{B}}$ and $\bar{\mathbf{C}}$ can be represented as,

$$\mathbf{A} = \mathrm{Q}^{1/2} \bar{\mathbf{A}} \mathrm{Q}^{-1/2}, \quad \mathbf{B} = \mathrm{Q}^{1/2} \bar{\mathbf{B}} \mathrm{I_w}^{-1/2}, \quad \mathbf{C} = \mathrm{I_w}^{1/2} \bar{\mathbf{C}} \mathrm{Q}^{-1/2}, \tag{8}$$

and the discretized input $\bar{\mathbf{f}}$ and the output $\bar{\boldsymbol{\phi}}$ vectors are transformed to

$$\mathbf{f} = \mathrm{I_w}^{1/2} \bar{\mathbf{f}}, \quad \boldsymbol{\phi} = \mathrm{I_w}^{1/2} \bar{\boldsymbol{\phi}}. \tag{9}$$

With this change of coordinates the state-space representation in equation (4) can be rewritten as,

$$\begin{aligned} \frac{\mathrm{d}}{\mathrm{d}t}\mathbf{q} &= \mathbf{A}\mathbf{q} + \mathbf{B}\mathbf{f}, \\ \boldsymbol{\phi} &= \mathbf{C}\mathbf{q}, \end{aligned} \tag{10}$$

B. Second-order statistics in response to stochastic excitations

We next characterize the structural dependence between the second-order statistics of the state and forcing term in the linearized dynamics. We also describe how the energy amplification arising from persistent stochastic excitation and

Downloaded by University of Southern California on December 22, 2023 | http://arc.aiaa.org | DOI: 10.2514/6.2023-3709

the energetically dominant flow structures can be computed from these flow statistics. All mathematical statements in the remainder of this section are parameterized over homogeneous spanwise direction.

In boundary layer flows, the linearized flow system is globally stable. In order to model the stochastic sources of uncertainties such as surface roughness or free-stream turbulence encountered in hypersonic wind-tunnels, the external disturbance $\mathbf{f}$ in equation (10) are assumed to be zero-mean and white-in-time stochastic forcing with covariance $\mathbf{W} \succ \mathbf{0}$, i.e.,

$$\mathbb{E}\left(\mathbf{f}\left(t_1\right)\mathbf{f}^*\left(t_2\right)\right) \;=\; \mathbf{W}\delta\left(t_1 - t_2\right), \tag{11}$$

where δ is the Dirac delta function, $\mathbb{E}(\cdot)$ denotes the expectation operator, and * denotes the complex-conjugate-transpose. In the statistical steady state, the output covariance matrix at a given spanwise wavenumber k_z is given by $\mathbf{\Phi} = \lim_{t\to\infty}\mathbb{E}\left(\boldsymbol{\phi}(k_z,t)\boldsymbol{\phi}^*(k_z,t)\right)$ associated with the output vector $\boldsymbol{\phi}$, and it is related to the state covariance $\mathbf{X}(k_z) = \lim_{t\to\infty}\mathbb{E}\left(\mathbf{q}(k_z,t)\mathbf{q}^*(k_z,t)\right)$ via

$$\mathbf{\Phi} = \mathbf{C}\mathbf{X}\mathbf{C}^*. \tag{12}$$

The steady state covariance $\mathbf{X}$ of the state $\mathbf{q}$ is determined by the solution to the Lyapunov equation,

$$\mathbf{A}\mathbf{X} + \mathbf{X}\mathbf{A}^* = -\mathbf{B}\mathbf{W}\mathbf{B}^*. \tag{13}$$

The Lyapunov equation (13) relates the statistics of white-in-time forcing, represented by $\mathbf{W}$, to the infinite-horizon state covariance $\mathbf{X}$ via system matrices $\mathbf{A}$ and $\mathbf{B}$. It can also be used to compute the energy spectrum associated with the output fluctuations $\boldsymbol{\phi}$,

$$E = \mathrm{trace}(\mathbf{\Phi}) = \mathrm{trace}\left(\mathbf{C}\mathbf{X}\mathbf{C}^*\right). \tag{14}$$

We note that the steady-state output covariance matrix $\mathbf{\Phi}$ can be alternatively obtained from the spectral density matrix of output fluctuations $S_{\boldsymbol{\phi}}$ as [36],

$$S_{\boldsymbol{\phi}}(\omega) \;:=\; T_{\phi\mathbf{f}}(\omega)\,\mathbf{W}\,T^*_{\phi\mathbf{f}}(\omega) \tag{15}$$

where the frequency response matrix

$$T_{\phi\mathbf{f}}(\omega) \;=\; \mathbf{C}\left(\mathrm{i}\omega\mathbf{I} - \mathbf{A}\right)^{-1}\mathbf{B}, \tag{16}$$

is obtained by applying the temporal Fourier transform on system (10). We note that the solution $\mathbf{X}$ to the algebraic Lyapunov equation (13) allows us to avoid integration over temporal frequencies and compute the energy spectrum E using (14).

III. Local analysis of stochastically forced stagnation point flow

To analyze the response of hypersonic blunt body flows to small external disturbances, we first quantify the linear amplification near the stagnation region. The objective of this section is to characterize the role of important physical parameters such as wall temperature and the radius of curvature on this amplification. For the rest of this section, we will utilize the local boundary layer profile close to the stagnation location and assume that this flow profile is invariant in the streamwise direction.

A. Stagnation boundary layer flow

The stagnation boundary layer profile is obtained by utilizing the local similarity method. The Levy-Lees-Dorodnitsyn transformations is applied, i.e.,

$$\begin{aligned} \xi &:= \int_0^{x_w} \rho_2 u_2 \mu_2 \,\mathrm{d}x, \\ \eta &:= \frac{u_2}{\sqrt{2\xi}} \int_0^{y_w} \rho \,\mathrm{d}y, \end{aligned} \tag{17}$$

Downloaded by University of Southern California on December 22, 2023 | http://arc.aiaa.org | DOI: 10.2514/6.2023-3709

Table 1 Free-stream conditions for local analysis

M_∞	T_∞	U_∞	ρ_∞
10	227 K	3000 m/s	0.01 Kg/m^3

where the coordinate x_w is measured from the stagnation location along the surface and the coordinate y_w is measured orthogonal to the body surface. The introduction of transformations in equation (17), allows us to look for similarity solutions [1],

$$f' = f'(\eta) = \frac{u}{u_e}, \quad g = g(\eta) = \frac{T}{T_e}, \tag{18}$$

where, u_e and T_e denote the velocity and the temperature at the edge of the boundary layer. In the present case, we utilize the pressure distribution from modified Newtonian theory and assumption of isentropic flow along the surface to obtain these flow parameters along the edge of the boundary layer. Note that, even though the base flow varies along the coordinates (x_w, y_w), it is only a function of η in the transformed coordinates. As a result, the non-dimensional stagnation boundary layer equations can be expressed as coupled ordinary differential equations (ODEs),

$$\begin{aligned} (Cf'')' + ff'' &= (f')^2 - g, \\ \left(\frac{C}{Pr}g'\right)' + fg' &= 0, \end{aligned} \tag{19}$$

where, Pr denotes the Prandtl number of the gas. In general, the variable C also depends on the properties of the gas and the pressure variation along the blunt body. However, for the present work, we assume that the gas of interest is air with constant $Pr \approx 0.72$. Furthermore, the pressure across the stagnation point can be well approximated as constant which allows us to express $C = g^{-0.28}$ and $\rho = \rho_e T_e / T$. The ODEs in the equation (19) are accompanied by the following boundary conditions,

$$\begin{aligned} &\text{at } \eta = 0 \text{ (wall)}, \ f = f' = 0; g = g_w, \\ &\text{at } \eta \to \infty \text{ (region-2)}, \ f' = 1; g = 1, \end{aligned} \tag{20}$$

where $g_w := T_w/T_e$ is the ratio of wall temperature to the temperature in the region-2. Physically, the values of the boundary condition $g_w \in (0, 1]$. For example, $g_w = 1$ implies a surface which is in thermal equilibrium with the stagnated flow, while $g_w < 1$ signifies a surface which is cooler than the surrounding fluid. Equation (20) illustrates that the value of g_w together with the leading edge radius $\mathcal{R}$ serve as the two parameters in the blunt-body flow.

B. Energy amplification in a stagnation boundary layer flow

In what follows, we utilize the analysis presented in the section II to quantify energy amplification in the presence of external stochastic forcing in a hypersonic blunt body flow. For carrying out the local analysis, we assume that the base flow profile is invariant in both the spanwise z and the streamwise x direction. As a result, we can utilize Fourier transform in both these directions and the state-space representation as described in equation (10) can be parameterized in terms of the spanwise wavenumber k_z and streamwise wavenumbers k_x. The velocity and the temperature are non-dimensionalized using the edge velocity U_e and edge temperature T_e, respectively. All the length scales are non-dimensionalized using the boundary layer scale $l := \sqrt{x_w \mu_e/(\rho_e U_e)}$, where x_w denotes the distance from the stagnation point along the surface.

In this section, we will assume that the external disturbances are associated with the sources of streamwise, wall-normal and spanwise momentum, i.e. $\mathbf{d}(\mathbf{x}, t) := (\hat{d}_x(y,t), \hat{d}_y(y,t), \hat{d}_z(y,t))e^{\mathrm{i}(k_x x + k_z z)}$. Furthermore, these disturbances are assumed to have unit covariance in space and input matrix $\mathbf{B}$ in equation (10) is chosen such that these disturbances are introduced uniformly throughout the wall normal direction. To make the discussions in this section concrete we choose the dimensional free-stream conditions as shown in table 1. Furthermore, we assume a fixed angular location of $\varphi = 5^\circ$ from the stagnation point (the angle of attack is fixed at 0°) for all the results presented in this section. For carrying out the local analysis we utilize a Chebyshev polynomial based discretization. The linearized dynamics are approximated numerically using 150 Chebyshev collocation points over a wall normal extent $L = 75$. By increasing the number of points it is confirmed that this resolution is high enough. We also find that the energy of the steady of state response is insensitive to any further increase in the wall normal height L.

Downloaded by University of Southern California on December 22, 2023 | http://arc.aiaa.org | DOI: 10.2514/6.2023-3709

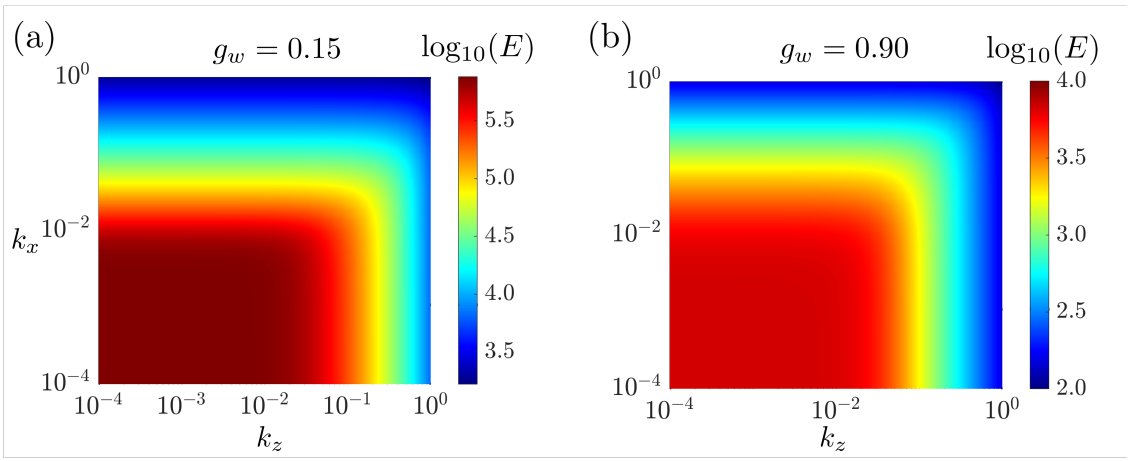

Fig. 2 Plots of $\log_{10}(E(\mathbf{k}))$ in the stagnation point boundary layer subject to white-in-time stochastic excitations at (a) cold wall $g_w = 0.15$ and (b) hot wall $g_w = 0.9$. The Reynolds number based on blunt-body curvature $Re_n = 1.33 \times 10^3$.

Figure 2 shows the energy E associated with the statistical steady state response as a function of the wavenumbers (k_x, k_z) for a flow with a bluntness Reynolds number $Re_n = 1.33 \times 10^3$. Here, bluntness Reynolds number is defined in terms of leading edge radius of curvature $Re_n = \rho_e U_e \mathcal{R}/\mu_e$. As shown in the figure, below a certain spanwise and streamwise wavelength, there is a strong attenuation of the energy associated with the flow response. Even though this behavior is independent of the wall temperature, there are some important differences. In particular, in the flow with a colder wall (see figure 2 (a) with $g_w = 0.15$), the fluctuations undergo a much larger amplification than that observed in hotter wall as shown in figure 2 (b) with $g_w = 0.9$.

Figure 3 plots variation of the maximum energy $E_{\max}$ associated with the flow fluctuations that undergo the largest amplification (over k_x, k_z values) for a range of bluntness Reynolds number Re_n and wall temperature g_w. Figure 3 (a) shows that there is a considerable change in the overall growth of flow fluctuations as we vary Re_n and g_w. In particular, we note that as the wall-temperature increases, there is a significant decline in the fluctuation energy E. On the hand, an increase in the Re_n causes an increase in E regardless of the parameter g_w. These conclusions are in good agreement with flow experiments over blunt bodies in wind tunnels, where an increase in bluntness or a decrease in wall temperature causes the transition to turbulence to appear closer to the nose-tip [3, 4, 6, 7].

To make these observations quantitative figure 3 (b) plots $E_{\max}$ as a function of Re_n. As shown in the figure, over a cold wall, the energy of the fluctuations grows slightly faster than a quadratic function of Re_n (it goes as $O(Re_n^{2.4})$). On the other hand, at hot-wall conditions, the E exhibits a much smaller growth. At these conditions, we observe two distinct trends: at lower Re_n, the increase in energy is sub-linear, however, as the Reynolds number increases, it starts to approach a quadratic function of Re_n.

The main objective of this section has been to analyze the energy associated with the steady state response of hypersonic blunt body boundary layer in the presence of background noise. For this we have utilized a boundary layer profile close to the stagnation location. The local analysis which assumes spatial invariance in the streamwise and the spanwise directions indicates that in the presence of external stochastic disturbances, a decrease in the wall temperature and an increase in bluntness can significantly deteriorate the robustness of the laminar flow. Next, we analyze the role of convex curvature of the leading edge bluntness on the noise amplification by carrying out a global analysis in the presence of stochastic excitations near the leading edge.

IV. Global analysis of stochastically forced hypersonic flow over a blunt flat plate

The introduction of the bluntness in the leading edges has the positive effect of reducing the heat flux into the surface. Furthermore, it is also well known that increasing the bluntness can have an additional stabilizing effect for an intermediate range of leading edge/nose tip radius of curvature, delaying the laminar-turbulent transition further downstream along the surface. However, experiments indicate that this trend of delaying transition can be reversed beyond certain bluntness values, i.e. the transition front moves starts to move upstream leading to turbulence close to the leading

Downloaded by University of Southern California on December 22, 2023 | http://arc.aiaa.org | DOI: 10.2514/6.2023-3709

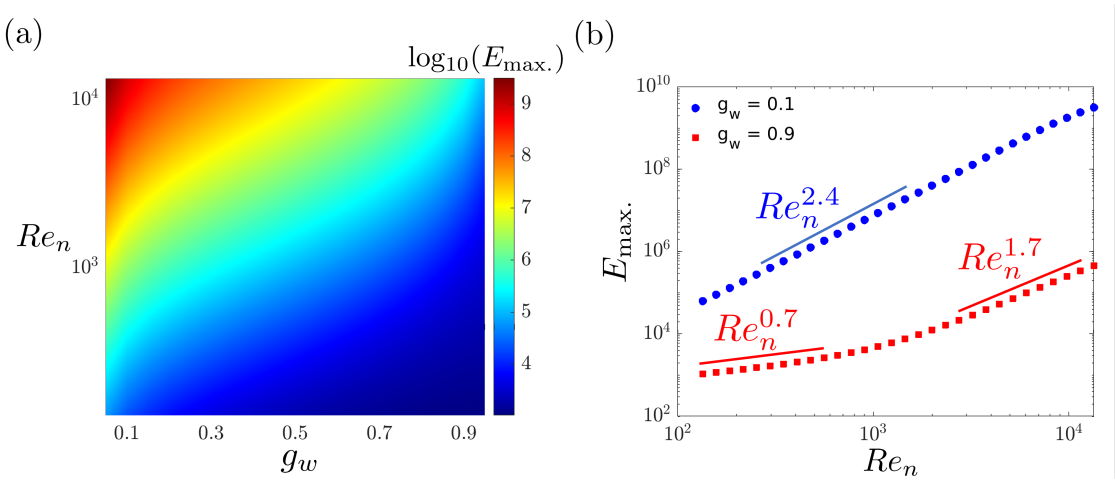

Fig. 3 Plots of maximum energy $\log_{10}(E_{\max.})$ as a function of wall temperature and leading edge bluntness Reynolds number.

Table 2 Free-stream conditions for global analysis

M_∞	T_∞	T_w	U_∞	ρ_∞
5	77.3 K	282K	881.2 m/s	0.338 Kg/m^3

edge or the nose-tip. This reversal in the onset of transition has been reported in numerous experiments [4, 6, 7, 13]. Although this 'transition-reversal' has been attributed to the presence of surface roughness near the stagnation location in experiments, quantifying the influence of such stochastic sources over such a rapidly spatially varying flow is still an open challenge. Herein, we employ the I/O framework to study the amplification of infinitesimal spanwise periodic stochastic excitation sources near the stagnation point in hypersonic blunt flat plate flow to investigate the transition reversal over a range of leading edge bluntness.

Recently, Borovoy et al. [13] report multiple hypersonic blunt flat plate experiments over a range of free-stream Reynolds number at Mach 5. Temperature sensitive paint measurements revealed that the transition reversal can be observed for a variety of bluntness profiles of the leading edge. Our objective is to quantify the noise amplification over cylindrical leading edges for which transition reversal is observed. In particular, we consider the experiments performed in the UT-1M Ludwig tube with a test time of 40 ms. As illustrated in the figure 4 (a), the geometry consists of total streamwise extent of $L = 6$ mm with a cylindrical profile of leading edge (the radius of the cylinder is denoted $\mathcal{R}$). This domain length is considerably shorter than the plate length in experiments. Our choice here is motivated by the desire to

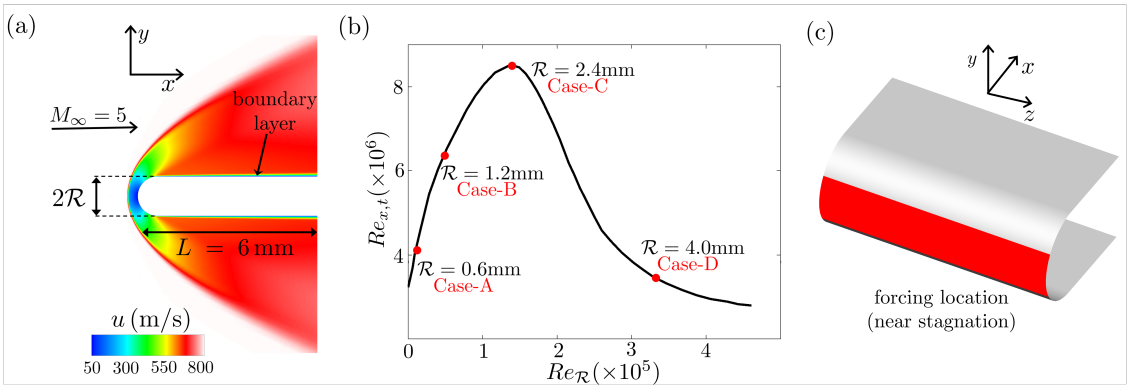

Fig. 4 (a) x-velocity over a flat plate with a blunt leading edge ($\mathcal{R} = 1.2$mm), (b) experimental data reproduced from Borovoy et al. [13], and (c) the spatial location for introducing the stochastic excitations.

Downloaded by University of Southern California on December 22, 2023 | http://arc.aiaa.org | DOI: 10.2514/6.2023-3709

investigate the dynamics close to the stagnation point and the flat plate leading edge junction. The experimental free stream conditions are reported in the table 2. Figure 4 (a) also provides the two-dimensional numerically computed flow field over a blunted flat plate with cylinder radius $\mathcal{R} = 1.2$mm. As shown in the figure, the presence of the curved leading edge introduces a strong normal shock and a considerable gradients close to the surface. As we move along the surface, the flow expands and accelerates along the shoulder near the flat plate cylinder junction causing the formation of a thin boundary layer profile while the free stream undergoes a substantial spatial variation in the streamwise direction. Figure 4 (b) reproduces the plot from experiments of Borovoy et al. [13]. This figure plots the variation of the Reynolds number at the onset of transition $Re_{x,t}$ against the Reynolds number based on the radius of curvature of the cylindrical leading edge $Re_{\mathcal{R}}$. This curve clearly shows the transition reversal observed in experiments over blunt bodies. The cylinder radii considered in the present work are also marked along this curve for reference.

A. Energy amplification in presence of stochastic sources near leading edge

We utilize the input-output analysis to investigate the amplification of infinitesimal upstream perturbations in the hypersonic blunt flat plate flow. In particular, we obtain the second order statistics associated with the flow response in the presence of the white-in-time excitation sources that are introduced near the leading edge. This choice of the forcing location is motivated by the experimental studies where the surface roughness near the leading edge is found to be an important factor in influencing the transition location downstream. In particular, we introduce stochastic excitations in the three momentum equations over a finite streamwise extent of 1mm and a wall normal extent of 2μm through a proper selection of the input matrix $\mathbf{B}$ (see figure 4 for illustration). This choice of forcing location is consistent across the range of leading edge radii considered in the present work.

The linearized dynamics as presented in the equations (10) are numerically approximated using a second order central finite volume based discretization. For the present flow configuration, we utilize 220 cells in the streamwise and 200 cells in the wall normal direction. The results presented in this section are found to be insensitive to further increase in the spatial resolution. Furthermore, we assume numerical sponges in the regions close to the leading edge around the stagnation point, towards the end of the flat plate and curved leading edge shock. In the present work, we are interested in quantifying the energy amplification that appears in different spatial regions of this flow. In particular, we want to quantify the amplification of flow fluctuations along the curved leading edge, and in the boundary layer on the flat plate using the matrix $\mathbf{C}$ in the equations (12).

B. A streaming algorithm for obtaining ensemble energy of flow fluctuations

The second order statistics associated with the response of the flow fluctuation can be obtained by solving the Lyapunov equations (13) and the resulting ensemble averaged energy associated with this response can be obtained by utilizing equation (14). The classical approaches for solving the Lyapunov equations computationally scale as $O(n^6)$, where n is the number of degrees of freedom associated with the state variable $\mathbf{q}$. As a result, these approaches are prohibitive for the current numerical resolution. To address this challenge, we utilize a streaming approach. Note that the solution $\mathbf{X}$ to equation (13) can also be expressed as [36],

$$\mathbf{X} \;=\; \int_0^\infty e^{\mathbf{A}t}\,\mathbf{B}\,\mathbf{W}\,\mathbf{B}^*\,e^{\mathbf{A}^*t}\,\mathrm{d}t, \tag{21}$$

where, * denotes complex conjugate transpose. For the present work we assume that the disturbance covariance is identity, i.e. $\mathbf{W} = \mathbf{I}$. Other non-diagonal covariances can be accounted in a straightforward manner. However, for the ease of presentation, we will assume that $\mathbf{W} = \mathbf{I}$ through out the rest of this work.

We can equivalently express equation (21) for the covariance matrix of the outputs as,

$$\mathbf{\Phi} \;=\; \sum_i \mathbf{C}\left(\int_0^\infty e^{\mathbf{A}t}\,b_i\,(e^{\mathbf{A}t}\,b_i)^*\,\mathrm{d}t\right)\mathbf{C}^*, \tag{22}$$

where, b_i denotes the i^{th} column of the input matrix $\mathbf{B}$. Therefore, in order to compute the trace of the output covariance

Downloaded by University of Southern California on December 22, 2023 | http://arc.aiaa.org | DOI: 10.2514/6.2023-3709

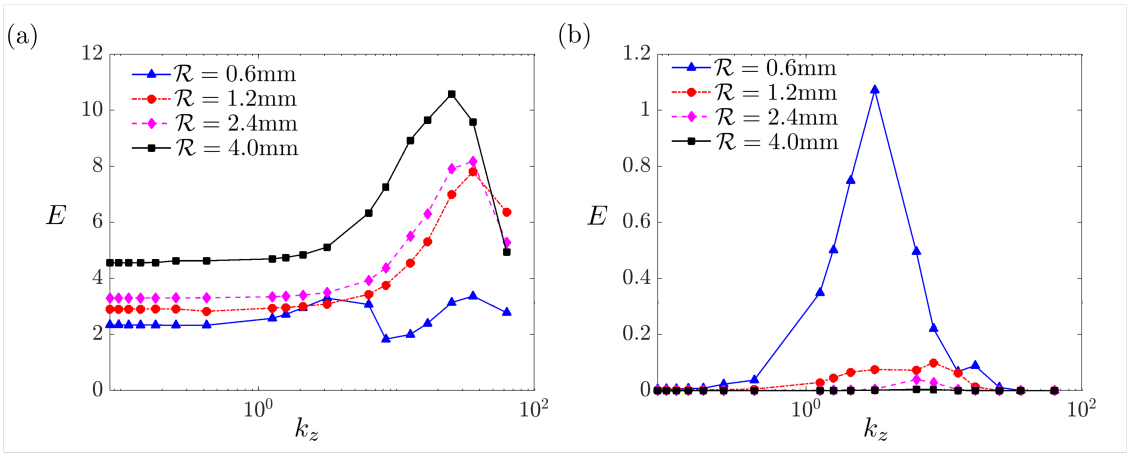

Fig. 5 Energy amplification over blunt leading edges over a range of radius of curvature $\mathcal{R}$: (a) near the stagnation region upstream of the flat plate, (b) in the boundary layer over the flat plate.

in equation (14), we utilize the following algorithm,

Data: **A**, **C**, **B**, bcols, maxiter, ϵ, timestep size Δt
Result: Γ which approximates tr($\mathbf{\Phi}$) in equation (14);
$\Gamma \leftarrow 0$;
$i \leftarrow 1$;
while $i <$ bcols **do**
  $k \leftarrow 1$;
  while $k <$ maxiter **do**
    $\phi_i \leftarrow 0$;
    $\nu_i \leftarrow b_i$;
    if $\|\nu_i\| > \epsilon$ **then**
      $\nu_i \leftarrow f(\mathbf{A}, \nu_i, \Delta t)$, where $f(\cdot)$ is function that updates ν_i over Δt;
      $\gamma_i \leftarrow \gamma_i + \Delta t\,(\mathbf{C}\nu_i)^*(\mathbf{C}\nu_i)$;
      $k \leftarrow k + 1$;
    else
      $i \leftarrow i + 1$;
    end
  end
  $\Gamma \leftarrow \Gamma + \gamma_i$;
end

Algorithm 1: Streaming algorithm for ensemble energy of the output fluctuations

Here, bcols refer to the number of columns in the forcing matrix **B**. The above algorithm can be trivially parallelized. In the present paper, we utilize explicit third-order Runge–Kutta scheme with a Courant–Friedrichs–Lewy number of 0.9.

C. Results

In this section, we quantify the energy of the flow fluctuations that emerge as a response to spatially localized stochastic excitation sources that are introduced close to the leading edge of the blunt flat plate. Physically, these disturbances can be thought of as modeling the influence of small randomly distributed roughness near the stagnation point. Here, we make sure that these disturbances are restricted to roughly 1% of the stagnation boundary layer thickness in the wall normal direction and ≈ 2 times the stagnation boundary layer thickness in the streamwise direction for all the leading edge bluntness described in the previous sections.

The homogeneity of the base flow in the spanwise direction allows us to parameterize the dynamics in terms of spanwise wavenumber k_z. For each of the cylindrical leading edge (as marked in figure 4 (b)), we utilize the algorithm 1

Downloaded by University of Southern California on December 22, 2023 | http://arc.aiaa.org | DOI: 10.2514/6.2023-3709

to compute the ensemble compressible energy (as defined in equation (6)) associated with the flow fluctuations. To quantify the relative amplification that appears in the stagnation region versus what can be obtained in the boundary layer, we utilize the two different output matrices $\mathbf{C}$ in equation (10). In the first case, we modify the output in a manner that we only measure the energy of fluctuations in the region before the cylinder flat plate junction. In the second case, we measure the energy over the flat plate while ignoring its growth in the convex region of the flow. Figure 5 (a) and (b) compares the amplification in these two regions. This comparison shows that across all the cylinder radii, the amplification over the curved leading edge is substantially larger than that over the flat plate region. The small amplification over the flat plate region, especially in the presence of relatively sharp leading edge can be attributed to the small streamwise extent of the flat plate.

A closer inspection of the energy of the flow fluctuations over the leading edge in figure 5 (a) reveals that as the leading edge radius increases, there is a substantial increase in the fluctuation amplification across a range of spanwise wavenumbers k_z. This observation is consistent with previous works [9, 16] where the largest possible transient spatial amplification of fluctuation energy increases monotonically as one increases the radius of curvature of the blunt body. Our computations demonstrate that this trend of increasing fluctuation growth is observed even in the presence of close-wall-stochastic forcing. In contrast to the fluctuation energy in the vicinity of the leading edge, figure 5 (b) reveals that over the flat plate the largest amplification is associated with the blunt flat plate geometry with the sharpest leading edge. In fact, an increase in the leading edge radius causes the fluctuation energy to attenuate. This observation is consistent with traditional normal mode analysis [10], where the increase in bluntness causes a stabilization of the boundary layer. Our computations of the response to stochastic sources near the leading edge suggests that the amplification that appears close to the stagnation region might play an important role in transition at higher values of the bluntness, i.e. at higher values of $\mathcal{R}$.

V. Concluding remarks

The main objective of the present study has been to analyze the steady state response of hypersonic blunt body flows in the presence of background noise using an input-output approach. We carry out this analysis in two parts. In the first part, we utilize a model for the laminar flow near the stagnation point while neglecting any streamwise variation. By utilizing linearized compressible boundary layer equations, we have demonstrated that the background noise can undergo significant amplification over a range of streamwise and spanwise length scales. Furthermore, we have investigated dependence of the steady state response on important physical parameters which are often used to control the behavior of the laminar blunt body flows. Our analysis indicates that in the presence of external stochastic disturbances, a decrease in the wall temperature and an increase in bluntness can significantly deteriorate the robustness of the laminar flow. In the second part of this paper, we utilize spatially evolving flow over flat plates with cylindrical leading edges. In this case, our analysis demonstrates that spatially localized background noise close to the surface of the leading edge can undergo substantial amplification over a range of spanwise length scales near the stagnation region. The point of view adopted in the present work quantifies the influence of uncertainties within an input-output framework and the observations from our analysis are found to agree well with the experimental trends. The present work provides the first steps towards developing control oriented models for flow transition in hypersonic flows. We expect that our work will motivate additional studies for predictive modeling and control of transition to turbulence in high speed flows.

References

[1] White, F. M., and Majdalani, J., *Viscous fluid flow*, Vol. 3, McGraw-Hill New York, 2006.

[2] Van Driest, E. R., *The problem of aerodynamic heating*, Institute of the Aeronautical Sciences, 1956.

[3] Dunlap, R., and Kuethe, A. M., "Effects of cooling on boundary-layer transition on a hemisphere in simulated hypersonic flow," *J. Aero. Sc.*, Vol. 29, No. 12, 1962, pp. 1454–1461.

[4] Stetson, K., "Nosetip bluntness effects on cone frustum boundary layer transition in hypersonic flow," *16th Fluid Plasma Dynamics Conference*, 1983, p. 1763.

[5] Reshotko, E., "Transition issues for atmospheric entry," *J. Spacecr. Rockets*, Vol. 45, No. 2, 2008, pp. 161–164.

[6] Lysenko, V., "Influence of the entropy layer on the stability of a supersonic shock layer and transition of the laminar boundary layer to turbulence," *J. App. Mech. Tech. Physics*, Vol. 31, No. 6, 1990, pp. 868–873.

Downloaded by University of Southern California on December 22, 2023 | http://arc.aiaa.org | DOI: 10.2514/6.2023-3709

[7] Jewell, J. S., Kennedy, R. E., Laurence, S. J., and Kimmel, R. L., "Transition on a variable bluntness 7-degree cone at high Reynolds number," *2018 AIAA Aerospace Sciences Meeting*, 2018, p. 1822.

[8] Reshotko, E., "Transient growth: a factor in bypass transition," *Phys. Fluids*, Vol. 13, No. 5, 2001, pp. 1067–1075.

[9] Paredes, P., Choudhari, M. M., Li, F., Jewell, J. S., Kimmel, R. L., Marineau, E. C., and Grossir, G., "Nosetip bluntness effects on transition at hypersonic speeds: experimental and numerical analysis under NATO STO AVT-240," *2018 AIAA Aerospace Sciences Meeting*, 2018, p. 0057.

[10] Mack, L. M., "Boundary-layer linear stability theory," *In AGARD, Special Course on Stability and Transition of Laminar Flow*, Vol. 1, 1984.

[11] Dietz, G., and Hein, S., "Entropy-layer instabilities over a blunted flat plate in supersonic flow," *Phys. Fluids*, Vol. 11, No. 1, 1999, pp. 7–9.

[12] Fedorov, A., and Tumin, A., "Evolution of disturbances in entropy layer on blunted plate in supersonic flow," *AIAA J.*, Vol. 42, No. 1, 2004, pp. 89–94.

[13] Borovoy, V. Y., Radchenko, V. N., Aleksandrov, S. V., and Mosharov, V. E., "Laminar–turbulent transition reversal on a blunted plate with various leading-edge shapes," *AIAA J.*, Vol. 60, No. 1, 2022, pp. 497–507.

[14] Trefethen, L. N., Trefethen, A. E., Reddy, S. C., and Driscoll, T. A., "Hydrodynamic stability without eigenvalues," *Science*, Vol. 261, No. 5121, 1993, pp. 578–584.

[15] Schmid, P. J., and Henningson, D. S., *Stability and transition in shear flows*, Springer-Verlag, New York, 2001.

[16] Reshotko, E., and Tumin, A., "The blunt body paradox—A case for transient growth," *Laminar-Turbulent Transition*, Springer, 2000, pp. 403–408.

[17] Paredes, P., Choudhari, M. M., and Li, F., "Blunt-body paradox and transient growth on a hypersonic spherical forebody," *Phys. Rev. Fluids*, Vol. 2, No. 5, 2017, p. 053903.

[18] Paredes, P., Choudhari, M. M., Li, F., Jewell, J. S., and Kimmel, R. L., "Nonmodal growth of traveling waves on blunt cones at hypersonic speeds," *AIAA J.*, Vol. 57, No. 11, 2019, pp. 4738–4749.

[19] Aleksandrova, E. A., Novikov, A. V., Utyuzhnikov, S. V., and Fedorov, A. V., "Experimental study of the laminar-turbulent transition on a blunt cone," *J. App. Mech. Tech. Phys.*, Vol. 55, 2014, pp. 375–385.

[20] Jovanović, M. R., "Modeling, analysis, and control of spatially distributed systems," Ph.D. thesis, University of California, Santa Barbara, 2004.

[21] Jovanović, M. R., and Bamieh, B., "Componentwise energy amplification in channel flows," *J. Fluid Mech.*, Vol. 534, 2005, pp. 145–183.

[22] Jovanović, M. R., "From bypass transition to flow control and data-driven turbulence modeling: An input-output viewpoint," *Annu. Rev. Fluid Mech.*, Vol. 53, No. 1, 2021, pp. 311–345.

[23] Brandt, L., Sipp, D., Pralits, J. O., and Marquet, O., "Effect of base-flow variation in noise amplifiers: the flat-plate boundary layer," *J. Fluid Mech.*, Vol. 687, 2011, pp. 503–528.

[24] Sipp, D., and Marquet, O., "Characterization of noise amplifiers with global singular modes: the case of the leading-edge flat-plate boundary layer," *Theoretical and Computational Fluid Dynamics*, Vol. 27, No. 5, 2013, pp. 617–635.

[25] Fosas de Pando, M., and Schmid, P. J., "Optimal frequency-response sensitivity of compressible flow over roughness elements," *J. Turbul.*, Vol. 18, No. 4, 2017, pp. 338–351.

[26] Ran, W., Zare, A., Hack, M. J. P., and Jovanović, M. R., "Stochastic receptivity analysis of boundary layer flow," *Phys. Rev. Fluids*, Vol. 4, No. 9, 2019, p. 093901 (28 pages).

[27] Jeun, J., Nichols, J. W., and Jovanović, M. R., "Input-output analysis of high-speed axisymmetric isothermal jet noise," *Phys. Fluids*, Vol. 28, No. 4, 2016, p. 047101 (20 pages).

[28] Dwivedi, A., Sidharth, G. S., Nichols, J. W., Candler, G. V., and Jovanović, M. R., "Reattachment vortices in hypersonic compression ramp flow: an input-output analysis," *J. Fluid Mech.*, Vol. 880, 2019, pp. 113–135.

Downloaded by University of Southern California on December 22, 2023 | http://arc.aiaa.org | DOI: 10.2514/6.2023-3709

[29] Dwivedi, A., Sidharth, G. S., Candler, G. V., Nichols, J. W., and Jovanović, M. R., "Input-output analysis of shock boundary layer interaction," *2018 Fluid Dynamics Conference*, 2018. AIAA 2018-3220.

[30] Dwivedi, A., Candler, G. V., and Jovanović, M. R., "A frequency domain analysis of compressible linearized Navier-Stokes equations in a hypersonic compression ramp flow," *Proceedings of the 2020 American Control Conference*, Denver, CO, 2020, pp. 4325–4330.

[31] Dwivedi, A., Sidharth, G. S., and Jovanović, M. R., "Oblique transition in hypersonic double-wedge flow," *J. Fluid Mech.*, Vol. 948, 2022.

[32] Candler, G. V., Johnson, H. B., Nompelis, I., Gidzak, V. M., Subbareddy, P. K., and Barnhardt, M., "Development of the US3D code for advanced compressible and reacting flow simulations," *53rd AIAA Aerospace Sciences Meeting*, 2015. AIAA 2015-1893.

[33] Sidharth, G. S., Dwivedi, A., Candler, G. V., and Nichols, J. W., "Onset of three-dimensionality in supersonic flow over a slender double wedge," *Phys. Rev. Fluids*, Vol. 3, No. 9, 2018, p. 093901.

[34] Schmid, P. J., "Nonmodal stability theory," *Annu. Rev. Fluid Mech.*, Vol. 39, 2007, pp. 129–162.

[35] Chu, B.-T., "On the energy transfer to small disturbances in fluid flow (Part I)," *Acta Mech.*, Vol. 1, No. 3, 1965, pp. 215–234.

[36] Kwakernaak, H., and Sivan, R., *Linear optimal control systems*, Vol. 1072, Wiley-interscience New York, 1969.

Downloaded by University of Southern California on December 22, 2023 | http://arc.aiaa.org | DOI: 10.2514/6.2023-3709